Journal of Power Sources 185 (2008) 1284–1292

Contents lists available at ScienceDirect

Journal of Power Sources

journal homepage: www.elsevier.com/locate/jpowsour

Analysis of a novel autonomous marine hybrid power generation/energy storage system with a high-voltage direct current link

Li Wang [a], Dong-Jing Lee [a,*], Wei-Jen Lee [b], Zhe Chen [c]

[a] Department of Electrical Engineering, National Cheng Kung University, Tainan city 701, Taiwan, ROC
[b] Department of Electrical Engineering, University of Texas at Arlington (UTA), Arlington, TX 76019, USA
[c] Institute of Energy Technology (IET), Aalborg University, Analog, Denmark

ARTICLE INFO

Article history:
Received 16 June 2008
Received in revised form 12 August 2008
Accepted 20 August 2008
Available online 26 August 2008

Keywords:
Wave-energy turbine generators (WETGs)
Aqua electrolyzer (AE)
Fuel cells (FCs)
Diesel-engine generators (DEGs)
Compressed air energy storage system (CAES)
Flywheel energy storage system (FESS)

ABSTRACT

This paper presents both time-domain and frequency-domain simulated results of a novel marine hybrid renewable-energy power generation/energy storage system (PG/ESS) feeding isolated loads through an high-voltage direct current (HVDC) link. The studied marine PG subsystems comprise both offshore wind turbines and Wells turbines to respectively capture wind energy and wave energy from marine wind and ocean wave. In addition to wind-turbine generators (WTGs) and wave-energy turbine generators (WETGs) employed in the studied system, diesel-engine generators (DEGs) and an aqua electrolyzer (AE) absorbing a part of generated energy from WTGs and WETGs to generate available hydrogen for fuel cells (FCs) are also included in the PG subsystems. The ES subsystems consist of a flywheel energy storage system (FESS) and a compressed air energy storage (CAES) system to balance the required energy in the hybrid PG/ESS. It can be concluded from the simulation results that the proposed hybrid marine PG/ESS feeding isolated loads can stably operate to achieve system power-frequency balance condition.

1. Introduction

Marine renewable energy such as tidal current, offshore wind energy, wave energy, etc., will come to the market in a near future in Europe. The commitment of most of the countries in Europe can supply a large part of their energy to the loads from renewable-energy resources by 2010. The coupling of such intermittent sources with local energy storage systems is often necessary in order to regulate the energy output flow between power generation systems and connected loads. Energy demand in isolated small islands is steadily increasing and hence, it is very important to find some new schemes to meet the continually increasing demand of power in isolated small islands. One of the solutions for these issues is to integrate different forms of renewable energy.

A hybrid power generation/energy storage system (PG/ESS) may combine all different kinds of available renewable-energy associated with available energy storage units. The required power for the connected loads can be effectively delivered and supplied by a hybrid PG/ESS with appropriate control and effective coordination among various subsystems. Attractive locations for future large turbines would be remote, such as offshore, where wind conditions can be improved and planning restrictions can be reduced. Due to environmental concerns and planning limitations, most high-capacity wind farms are planned to install offshore. To transmit bulk generated power over long distances creates challenges for both system operators and wind-farm developers. Currently, there are two alternative methods for connecting remote wind farms to the grid, i.e., a high-voltage direct current (HVDC) link and a high-voltage alternating current (HVAC) line. The HVAC line is an economic solution for medium-range wind farms (up to a few hundred megawatts) with transmission distances less than 50–75 km [1–3].

On the other hand, hydrogen has attracted more attention in recent years because of the lack of fossil fuel and environmental pollution. Thus, aqua electrolyzer (AE) plants and fuel cells (FCs) have received increasing attention recently. The characteristics of FCs are quite different from the ones of traditional thermal power plants. FCs may generate electricity with the advantages of high efficiency, low pollution, onsite installation, reusability of exhaust heat and water, diversity of fuels, etc. [4–13].

The ESS plays an important role in a hybrid system to perform both functions of storing and releasing energy at an adequate time. A flywheel energy storage system (FESS) systematically stores an electric energy by means of kinetic energy through a rotating flywheel. The advantages of a FESS are high stored energy density, high power exchange with the system, high conversion efficiency of 80–90%, and long-lived pollution-free design [14]. As in many

* Corresponding authors. Tel.: +886 6 275 7575 62361; fax: +886 6 2763883.
E-mail address: n2893118@ccmail.ncku.edu.tw (D.-J. Lee).

0378-7753/$ – see front matter © 2008 Elsevier B.V. All rights reserved.
doi:10.1016/j.jpowsour.2008.08.037

Nomenclature

Δf	system frequency deviation
K	gain
P_s	total power generation to the system
P_s^*	command of average power absorbed by loads
P_t	net power of WTGs and WETGs to the system
P_T	net total power of both WTGs and WETGs
T	time constant
V_A	axial velocity of Wells turbine in m s^{-1}
V_W	wind speed of wind turbine in m s^{-1}

Abbreviations or subscripts

AE	quantities of aqua electrolyzer
CAES	quantities of compressed air energy storage system
DEG	quantities of diesel-engine generator
FC	quantities of fuel cells
FESS	quantities of flywheel energy storage system
HVAC	quantities of high-voltage alternating current
HVDC	quantities of high-voltage direct current
PG/ESS	power generation/energy storage system
WETG	quantities of wave-energy turbine generator
WTG	quantities of wind-turbine generator

countries, the potentials of installing new hydro-storage plants with pumping facilities are limited and many other energy storage devices are far from being economic. A compressed air energy storage (CAES) system may be an attractive investment opportunity for such purposes [15]. The surplus power in a system can be used to compress air to store in a cavern as potential energy and expanded at times of peak demand in a turbine.

Combining the above-mentioned different renewable-energy resources with different ES units and standby diesel-engine generators (DEGs) in a hybrid system, the generated electric energy can be effective distributed and controlled to meet the energy requirement of the connected loads. The generated intermittent electric energy from wind-turbine generators (WTGs) and wave-energy turbine generators (WETGs) can be used to resolve natural gas or water into hydrogen and oxygen using aqua electrolyzers. The generated hydrogen can then be compressed, stored, and transported to FCs through pipelines [16]. The above hybrid PG/ESS with WTG–WETG–FC/FESS–BESS as well as DEGs and an AE has exhibited several advantages to control electrical energy absorbed by the connected loads [16–24].

This paper is organized as follows. Section 2 describes the configuration and the employed models for the proposed hybrid PG/ESS with WTGs–WETGs–FCs/FESS–CAES as well as DEGs and an AE. Section 3 presents block diagrams for two studied cases of the proposed hybrid system. Sections 4 and 5 respectively analyze time-domain simulated results of the two cases under various values of wind speed and loading demand. Section 6 analyzes frequency-domain simulated results of the two studied cases with and without the HVDC link. Specific conclusions are drawn in Section 7.

2. Configuration of the proposed hybrid system

The configuration of the proposed hybrid marine renewable-energy PG/ESS is shown in Fig. 1. The PG subsystems comprise multiple WTGs, WETGs, FCs, and DEGs. The AE in Fig. 1 is employed to convert a part of the generated energy from WTGs and WETGs into available hydrogen to offer the required fuel for the FCs. The ES subsystems include a compressed air energy storage system and a flywheel energy storage system. Both CAES and FESS are connected to the load side and they are assumed to have enough capacity to store surplus energy generated by the PG subsystems. When the load demand increases, the CAES and the FESS can release enough energy to the connected loads within a very short time. The DEGs are standby generators that may automatically start up and connect to the system to deliver required power to the loads only when the total generated power of the WTGs, the WETGs, and/or the FCs is insufficient even if the CAES and/or the FESS may have enough stored energy.

The net power generation P_s shown in Fig. 1 is determined by: (a) a part of the output power from the WTGs (P_{WTG}) and the WETGs (P_{WETG}), (b) the output power of the DEGs (P_{DEG}), (c) the output power of DC–AC converter connected to the FCs (P_{FC}), (d) the exchanged power of the FESS (P_{FESS}), and (e) the exchanged power of the CAES (P_{CAES}). The expression of P_s can be expressed by

$$P_s = P_t + P_{DEG} + P_{FC} \pm P_{FESS} \pm P_{CAES} \quad (1)$$

in which

$$P_t = K_n(P_{WTG} + P_{WETG}) = P_{HVDC} - P_{AE} \quad (2)$$

is the net power generated from both WTGs and WETGs through the HVDC link delivered to the system, P_{HVDC} is the output power of a HVDC link, and K_n is the ratio of P_t to ($P_{WTG} + P_{WETG}$). Eq. (2) describes that the P_{AE} is obtained from a part of the total output power of both WTGs and WETGs using a controlled switch in front of the AE. The value of P_{AE} is not equal to P_{FC} since P_{FC} depends on several factors such as utilization factor, partial pressure of hydrogen and oxygen, flow rate of hydrogen, etc.

To precisely simulate the dynamic behaviors of practical WTGs, WETGs, DEGs, FCs, AE, CAES, FESS, etc., high-order mathematical models with nonlinearity should be employed. However, these high-order models may include associated power conditioners and controllers. For large-scale power system simulations, simplified models or transfer functions are generally employed. Hence, the power losses and associated controllers of the PG and ES subsystems shown in Fig. 1 are not considered in this paper.

To simplify descriptions for the employed models of the subsystems shown in Fig. 1, the wind-speed model, characteristics of WTG's output power, and transfer functions of an AE and a FESS can be referred to [26]. Other employed models are depicted as below.

2.1. Characteristic of WETG's output power [12,13]

The output power in W of the studied WETG is determined by

$$P_{wav} = k_{Wells} \cdot C_t(V_A^2 + V_P^2) \quad (3)$$

where k_{Wells} is the torque coefficient, C_t is the turbine torque coefficient, V_A is the axial velocity of air through turbine, and V_P is peripheral velocity of turbine-blade of a typical Wells turbine for wave energy conversion system.

2.2. Transfer functions of various PG subsystems

The transfer functions of each studied WTG, WETG, FC, and DEG shown in Fig 1 are respectively represented by a first-order lag as below.

$$G_{WTG_k}(s) = \frac{K_{WTG}}{1 + sT_{WTG}} = \frac{\Delta P_{WTG_k}}{\Delta P_W}, \quad k = 1, 2, \ldots, n \quad (4)$$

$$G_{WETG_k}(s) = \frac{K_{WETG}}{1 + sT_{WETG}} = \frac{\Delta P_{WETG_k}}{\Delta P_A}, \quad k = 1, 2, \ldots, n \quad (5)$$

$$G_{FC_k}(s) = \frac{K_{FC}}{1 + sT_{FC}} = \frac{\Delta P_{FC_k}}{\Delta P_{AE}}, \quad k = 1, 2, \ldots, n \quad (6)$$

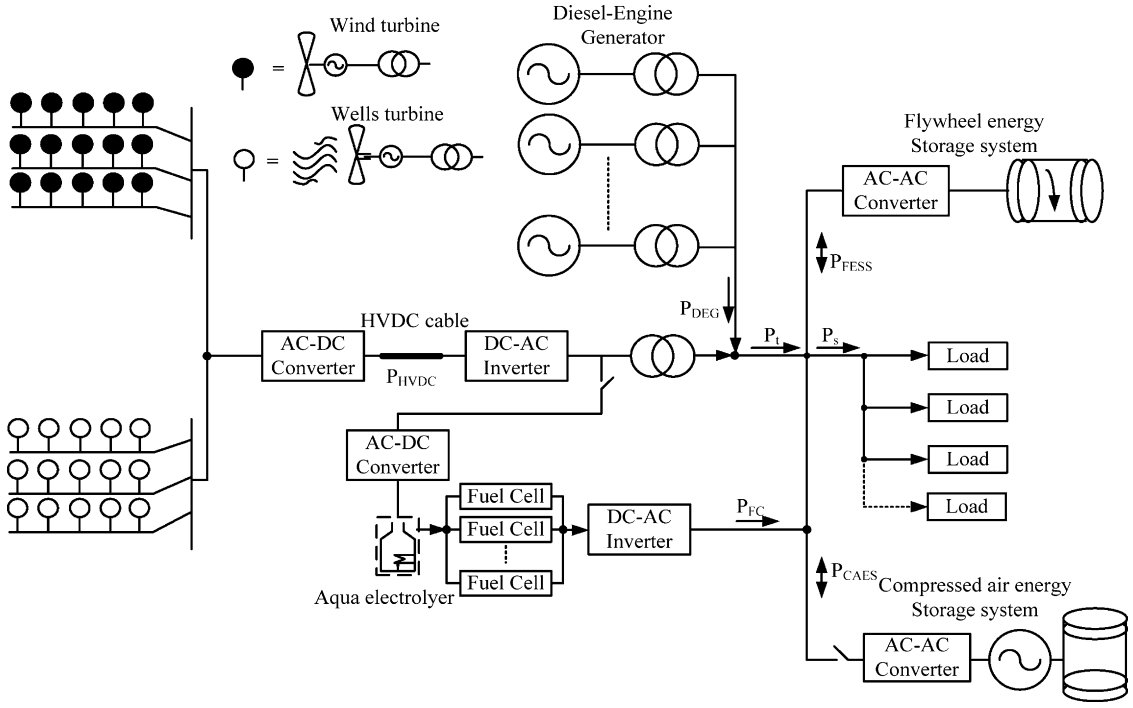

Fig. 1. Configuration of the studied marine hybrid PG/ESS.

$$G_{\mathrm{DEG}_k}(s) = \frac{K_{\mathrm{DEG}}}{1 + sT_{\mathrm{DEG}}} = \frac{\Delta P_{\mathrm{DEG}_k}}{\Delta f}, \quad k = 1, 2, \ldots, n \tag{7}$$

where P_{W} is mechanical input power of a WTG, P_{A} is mechanical input power of a WETG, and n is the number of generator or equipment.

2.3. Transfer functions of a CAES and an HVDC link

ES subsystems also play an important role to effectively supply insufficient energy of PG subsystems within a very short time to maintain system stability. A CAES stores the energy in the form of kinetic energy and it has the ability to store surplus energy during off-peak periods and quickly release energy during peak loads [22,23,25]. The transfer function of the CAES in Fig. 1 can be expressed as a first-order lag as follows.

$$G_{\mathrm{CAES}}(s) = \frac{K_{\mathrm{CAES}}}{1 + sT_{\mathrm{CAES}}} = \frac{\Delta P_{\mathrm{CAES}}}{\Delta f} \tag{8}$$

The transfer function of the HVDC link shown in Fig. 1 can also be represented by a first-order lag as below [1].

$$G_{\mathrm{HVDC}}(s) = \frac{K_{\mathrm{HVDC}}}{1 + sT_{\mathrm{HVDC}}} = \frac{\Delta P_{\mathrm{HVDC}}}{(\Delta P_{\mathrm{WTG}} + \Delta P_{\mathrm{WETG}})} \tag{9}$$

2.4. Power deviation and system frequency variation

To maintain a stable operation of an autonomous system, the total power generation must be effectively controlled to meet the total power demand of the connected loads. This power-control strategy is determined by the difference between power-demand reference P_{s}^* and total power generation P_{s} as follows.

$$\Delta P_{\mathrm{e}} = P_{\mathrm{s}}^* - P_{\mathrm{s}} \tag{10}$$

Since system frequency is changed with net power variation, the system frequency variation Δf is calculated by

$$\Delta f = \frac{\Delta P_{\mathrm{e}}}{K_{\mathrm{sys}}} = \frac{P_{\mathrm{s}}^* - P_{\mathrm{s}}}{K_{\mathrm{sys}}} \tag{11}$$

where K_{sys} is system-frequency characteristic constant of the hybrid PG/ESS. The transfer function for system frequency variation to per-unit power deviation can be expressed by

$$G_{\mathrm{sys}}(s) = \frac{\Delta f}{\Delta P_{\mathrm{e}}} = \frac{1}{K_{\mathrm{sys}}(1 + sT_{\mathrm{sys}})} = \frac{1}{D + Ms} \tag{12}$$

where M and D are respectively the equivalent inertia constant and damping constant of the hybrid PG/ESS [16,26].

3. Case studied of the proposed hybrid PG/ESS

This section presents two studied cases for evaluating performance of the proposed marine hybrid PG/ESS. The WTGs and WETGs in each case are random renewable sources to combine with the DEGs, the AE, the FCs, the FESS, and/or the CAES in Fig. 1. Power converters of the studied PG/ESS can properly operated with various PG and ES subsystems to perform required energy conversion. The DEGs can automatically start up to connect to the system in order to balance the power-demand variation of the connected loads. The employed parameters of the studied PG/ESS are listed in Table 1. The model parameters are determined by the cited papers [1,12,13,16,22,23,26] and the stability reference book [25]. These parameters have also considered practical operating conditions and characteristics of different subsystems. When the model

Table 1
Parameters of the studied hybrid marine PG/ESS

$K_{\mathrm{WTG}} = 1.0$ and $T_{\mathrm{WTG}} = 1.5$ s	$K_{\mathrm{WETG}} = 1.0$ and $T_{\mathrm{WETG}} = 1.3$ s
$K_{\mathrm{AE}} = 1/500$ and $T_{\mathrm{AE}} = 0.5$ s	$K_{\mathrm{DEG}} = 1/300$ and $T_{\mathrm{DEG}} = 2$ s
$K_{\mathrm{FC}} = 1/100$ and $T_{\mathrm{FC}} = 4$ s	$K_{\mathrm{CAES}} = -1/100$ and $T_{\mathrm{CAES}} = 0.1$ s
$K_{\mathrm{n}} = 0.6$, $M = 0.2$, and $D = 0.012$	$K_{\mathrm{FESS}} = -1/100$ and $T_{\mathrm{FESS}} = 0.1$ s
$K_{\mathrm{HVDC}} = 1/200$ and $T_{\mathrm{HVDC}} = 0.7$ s	

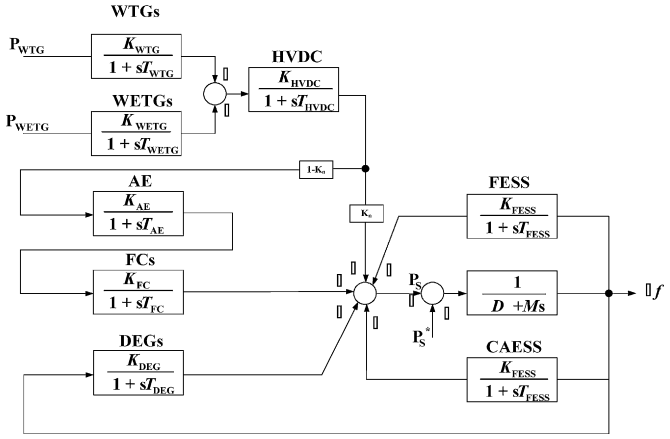

Fig. 2. Block diagram of the studied Case 1.

parameters are initially selected, they must be substituted into the developed mathematical model through both frequency-domain tests and time-domain tests. After the tests can meet the fundamental stability-analysis requirements, the adequate model parameters can be employed for system simulations. The block diagrams for the two studied cases are shown in Figs. 2 and 3 [16] and are described in the following two subsections, respectively.

3.1. Case 1

Fig. 2 shows the block diagram of Case 1. This case assumes that both WTGs and WETGs are connected to the system and they are operated together to respectively generate power P_{WTG} and P_{WETG}. A part of generated power from both WTGs and WETGs, i.e., $(1-K_n)(P_{WTG}+P_{WETG})$, is delivered to the AE to produce available hydrogen for the FCs. The FCs can generate DC power that is converted to an AC power P_{FC} using the DC–AC power inverter in Fig. 1. The P_{FC} is combined with P_{DEG} and P_t to supply average power to the connected loads. The surplus (insufficient) power of the studied hybrid system is properly stored in (released from) FESS and CAES through associated power converters. The net power generation of this case can be expressed by

$$P_s = P_{HVDC} - P_{AE} + P_{DEG} + P_{FC} \pm P_{FESS} \pm P_{CAES} \quad (13)$$

3.2. Case 2

Fig. 3 shows the block diagram of Case 2. This case assumes that the WTGs and the WETGs are respectively connected to the system at different times while the AE and the FCs are removed from the system. The power respectively generated by the WTGs (P_{WTG}) and the WETGs (P_{WETG}) is combined with P_{DEG} to supply required power demand of the connected loads. The surplus (insufficient) power of the studied hybrid system is properly stored in (released from) FESS and CAES through associated power converters. The net power generation of this case can be expressed by

$$P_s = P_{HVDC} + P_{DEG} \pm P_{FESS} \pm P_{CAES} \quad (14)$$

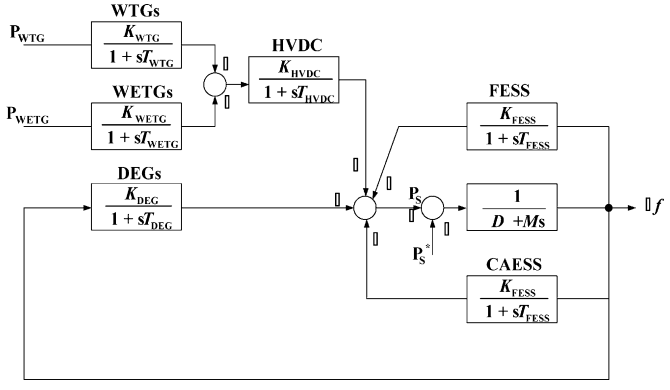

Fig. 3. Block diagram of the studied Case 2.

In these two cases, the average wind speed V_W of WTG is set to be around 7.5–15 m s^{-1} and the axial velocity V_A of air through WETGs is set to be ±5 m s^{-1}. The total demand power absorbed by the connected loads in the two studied cases is assumed to be $P_s^* = 1.0$ pu under normal operating condition. To deeply examine the effects of power-demand variation of connected loads and practical variable wind speeds of WTGs on dynamic performance of the studied hybrid PG/ESS, sudden drop and sudden rise of P_s^* and V_W are properly applied to the studied system at specified times.

4. Time-domain simulation results of Case 1

In this section, time-domain simulated responses of the studied marine hybrid PG/ESS under Case 1 are carried out. All quantities shown in the plots of this section are in per-unit value. Fig. 4 shows the time-domain simulated responses of Case 1. The dotted lines and solid lines shown in Fig. 4 are for the studied PG/ESS with an HVDC link and an HVAC line, respectively. The simulation results under different time intervals are respectively analyzed as below.

(1) *Base case*: When 0 s < t < 50 s, V_W is around 7.5 m s^{-1} and V_A is around ±5 m s^{-1}. The total average powers generated from WTGs and WETGs are: P_{WTG} is less than 0.5 pu and P_{WETG} is about 0.3 pu. A part of ($P_{WTG}+P_{WETG}$) is sent to the AE to generate P_{FC} of about 0.2 pu. Since WTGs and WETGs generate low power, DEGs automatically start up and connect to the system at t = 0 s so as to supply P_{DEG} of around 0.5 pu to compensate the load demand. No surplus energy can be stored in CAES and FESS due to low PG condition but Δf is varied slightly higher than zero.

(2) *Sudden load drop*: When 50 s < t < 100 s, V_W is still around 7.5 m s^{-1} but P_s suddenly drops from 1.0 to 0.5 pu at t = 50 s. Accordingly, P_{DEG} also drops from around 0.5 to 0.05 pu and Δf is varied slightly higher than zero.

(3) *Sudden load rise*: When 100 s < t < 200 s, V_W is around 7.5 m s^{-1} but P_s suddenly rises from 0.5 to 1.0 pu at t = 100 s. The responses are similar to the ones when 0 s < t < 50 s since the studied PG/ESS returns back to the same operating conditions of the base case.

(4) *Sudden drop of wind speed*: When 200 s < t < 300 s, V_W suddenly drops to close to the cut-in speed of WTG at t = 200 s and P_{WTG} decreases to around 0 pu but P_{WETG} is still around 0.3 pu. Since P_s is still kept at 1.0 pu, DEGs start up to generate P_{DEG} of around 0.7 pu. No surplus power can be stored in CAES and FESS and, hence, both P_{FESS} and P_{CAES} are equal to zero. It is seen that Δf is very close to zero since the total generated power just matches the required power demand of the connected loads.

(5) *Performance comparison of using HVDC and HVAC*: When 0 s < t < 300 s, the power of P_{WTG} and P_{WETG} are delivered to the connected load through an HVDC link. Since the power loss of an HVDC link is lower than the one of an HVAC line and, hence, the DEGs generate less power to the system when the HVDC link is in service. When 50 s < t < 100 s, both P_{FESS} and P_{CAES} can store less energy. It is obviously seen from Fig. 4 that the quantities of P_T, P_{AE}, P_{CELL}, and Δf for the system with the HVDC link are higher than the ones for the system with an HVAC line.

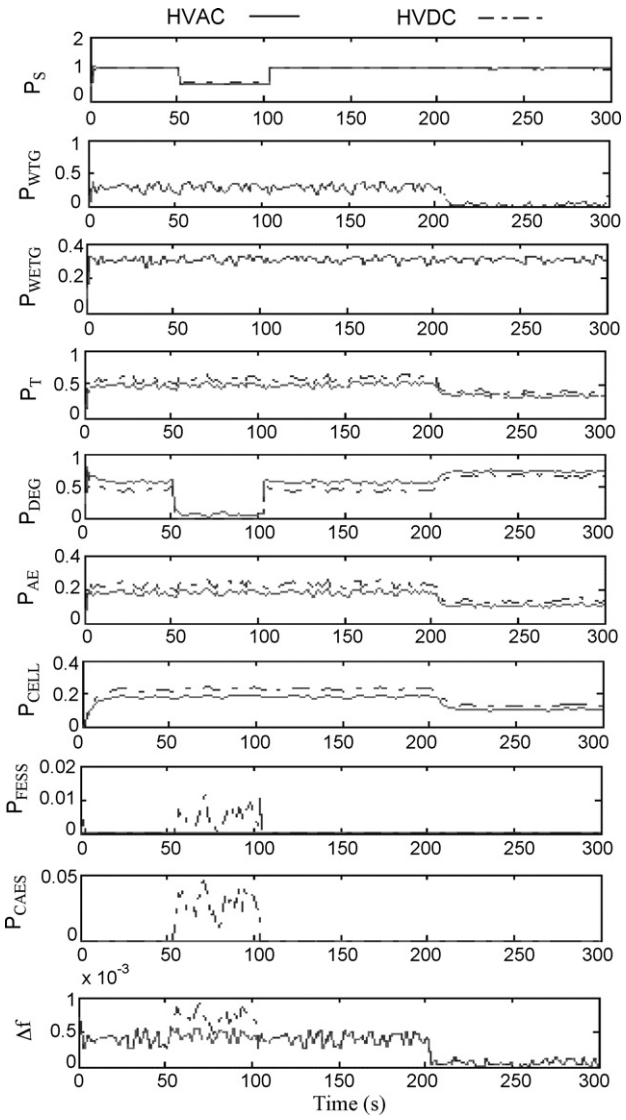

Fig. 4. Time-domain simulation results of Case 1.

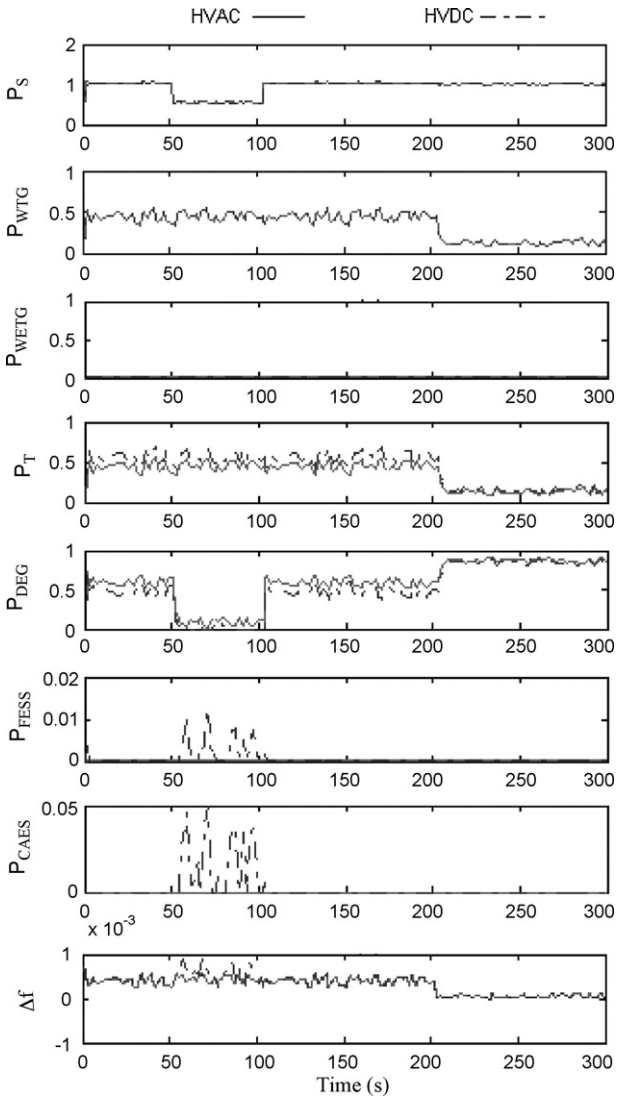

Fig. 5. Time-domain simulation results of Case 2 when only WTGs are connected to the system.

5. Time-domain simulation results of Case 2

The WTGs and WETGs in this case are respectively connected to the hybrid system at different specified times. To clearly compare the impact of the capacity of the WTGs on dynamic performance of the studied hybrid PG/ESS, this section is divided into four subsections. Fig. 5 (Fig. 6) shows the simulated results of the studied hybrid system containing WTGs (WETGs) only. The simulated results of the studied hybrid system with (without) both WTGs and WETGs connected to the system are shown in Fig. 7 (Fig. 8).

5.1. System with WTGs only

This subsection assumes only WTGs are connected to the system. The simulation results shown in Fig. 5 are analyzed as below.

(1) *Base case*: When $0\,s < t < 50\,s$, V_W is around $15\,m\,s^{-1}$ and P_{WTG} is around 0.5 pu but $P_{WTG} = 0$. The total generated power from WTGs is evidently not enough to supply the required load demand and, hence, DEGs start up and connect to the system at $t = 0\,s$. The DEGs generate P_{DEG} of about 0.5 pu to combine with P_{WTG} to meet the load demand. Approximate zero powers of P_{FESS} and P_{CAES} are released from FESS and CAES, respectively. Since the total generated power is close to the total load demand, Δf is slightly higher than zero.

(2) *Sudden load drop*: When $50\,s < t < 100\,s$, P_s drops from 1.0 to 0.5 pu at $t = 50\,s$ and P_{DEG} also drops to around 0.1 pu to meet the load demand. The surplus powers stored in FESS (P_{FESS}) and CAES (P_{CAES}) are around 0.01 and 0.05 pu, respectively. The system frequency deviation Δf is slightly higher than zero.

(3) *Sudden load rise*: When $100\,s < t < 200\,s$, P_s suddenly rises from 0.5 to 1.0 pu at $t = 100\,s$ and P_{DEG} also rises to around 0.5 pu to meet the load demand. The powers released from FESS (P_{FESS}) and CAES (P_{CAES}) are still close to zero and Δf is slightly higher than zero.

(4) *Sudden drop of wind speed*: When $200\,s < t < 300\,s$, V_W drops to a low speed at $t = 200\,s$ and P_{WTG} drops to close to 0.1 pu. To meet the required load demand, DEGs increase the total output power P_{DEG} to around 0.9 pu. No surplus power can be stored in FESS and CAES. Since the load demand can be supplied by the total generated power, Δf is close to zero.

(5) *Performance comparison of using HVDC and HVAC*: When $0\,s < t < 300\,s$, P_{WTG} is delivered to the connected loads through an HVDC link. The power flowing through the HVDC link is

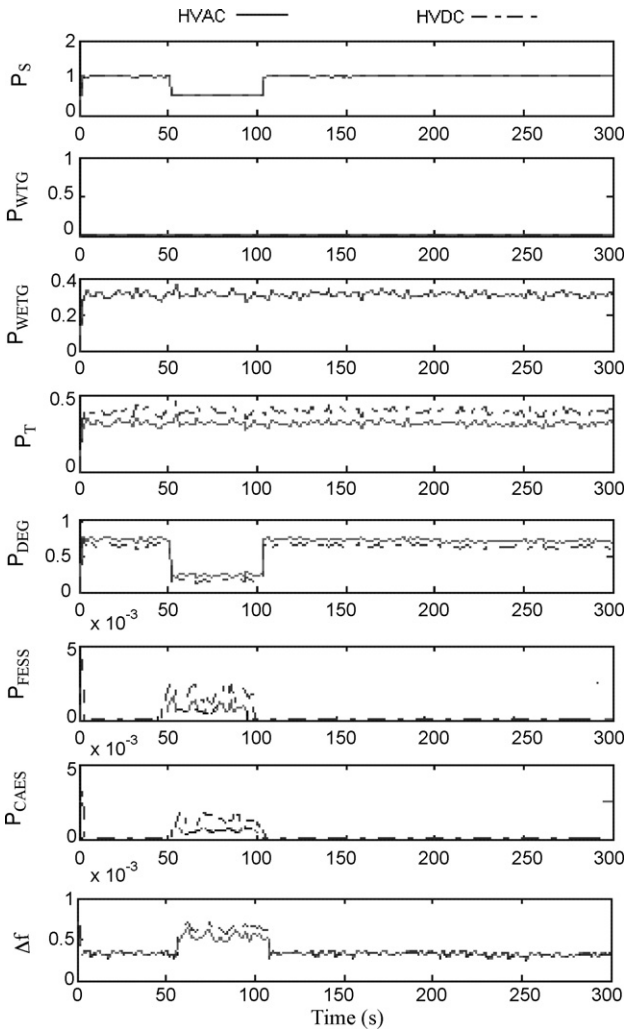

Fig. 6. Time-domain simulation results of Case 2 when only WETGs are connected to the system.

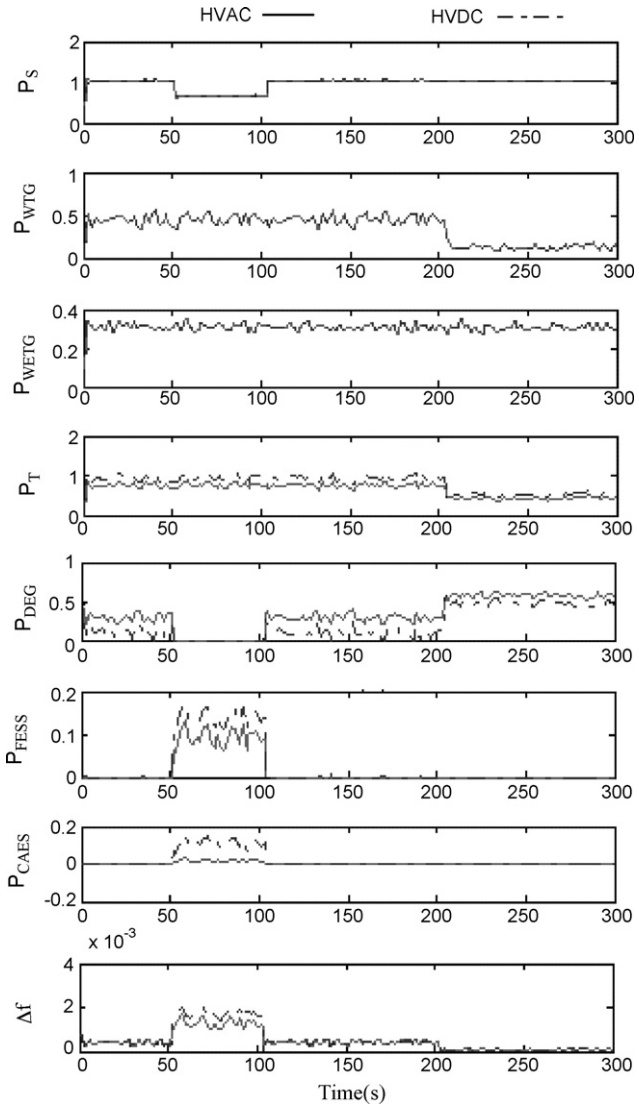

Fig. 7. Time-domain simulation results of Case 2 when both WETGs and WETGs are simultaneously connected to the system.

higher than the one through the HVAC line. Comparing with the HVAC line, the power flowing through the HVDC link may have less power loss. Hence, the DEGs may supply less power (P_{DEG}) to the system. When 50 s < t < 100 s, FESS and CAES can store more energy from the system with the HVDC link than the one with the HVAC line. It is obviously seen from Fig. 5 that the quantities of P_T and Δf for the system with the HVDC link are higher than the ones for the system with an HVAC line.

5.2. System with WETGs only

This subsection assumes only the WETGs are connected to the system. The time-domain simulation results shown in Fig. 6 are analyzed as below.

(1) *Base case*: When 0 s < t < 50 s, V_A is set to $\pm 5\ m\ s^{-1}$ and P_{WETG} is around 0.3 pu but P_{WTG} = 0 pu. The total generated power from WETGs is obviously not enough to supply the required load demand and, hence, DEGs start up and connect to the system at t = 0 s. The DEGs generate P_{DEG} of about 0.7 pu to combine with P_{WETG} to meet the load demand. Approximate zero powers of P_{FESS} and P_{CAES} are released from FESS and CAES, respectively. Since the total generated power is close to the total load demand, Δf is slightly higher than zero.

(2) *Sudden load drop*: When 50 s < t < 100 s, P_s drops from 1.0 to 0.5 pu at t = 50 s and P_{DEG} also drops to around 0.2 pu to meet the load demand. The system may store less surplus energy in FESS and CAES and Δf is slightly higher than zero.

(3) *Sudden load rise*: When 100 s < t < 300 s, P_s suddenly rises from 0.5 to 1.0 pu at t = 100 s and P_{DEG} also rises to around 0.7 pu to meet the load demand. The powers released from FESS (P_{FESS}) and CAES (P_{CAES}) are still close to zero. Again, Δf is slightly higher than zero.

(4) *Performance comparison of using HVDC and HVAC*: Since the power flowing through the HVDC link is higher than the one of the HVAC line, the HVDC link may have less power loss and the DEGs may generate less power to the system. It is obviously seen from Fig. 6 that the quantities of P_T, P_{FESS}, P_{CAES}, and Δf for the system with the HVDC link are higher than the ones for the system with an HVAC line.

5.3. System with both WTGs and WETGs

This subsection assumes both WTGs and WETGs are simultaneously connected to the system. The time-domain simulation results shown in Fig. 7 are analyzed as below.

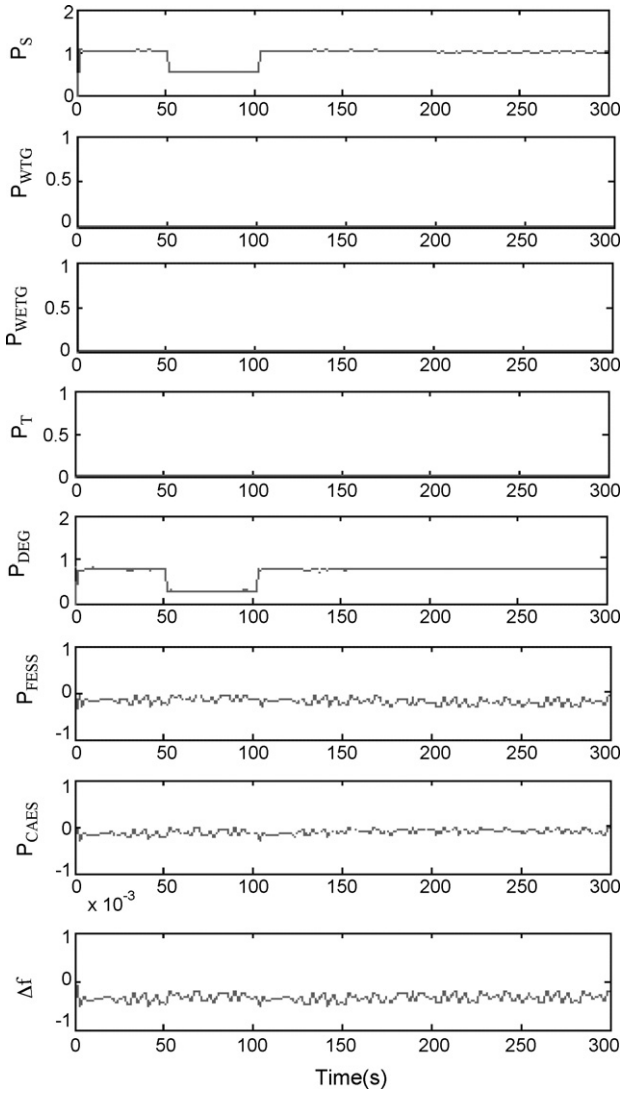

Fig. 8. Time-domain simulation results of Case 2 when both WETGs and WETGs are disconnected from the system.

(1) *Base case*: When $0\,s < t < 50\,s$, V_W is around $15\,m\,s^{-1}$, P_{WTG} is less than 0.5 pu, and P_{WETG} is about 0.3 pu. Since the low power is generated by both WTGs and WETGs, DEGs automatically start up and connect to the system at $t = 0\,s$ to supply P_{DEG} of around 0.25 pu. No surplus energy can be stored in CAES and FESS and Δf is varied slightly higher than zero.

(2) *Sudden load drop*: When $50\,s < t < 100\,s$, V_W is still around $7.5\,m\,s^{-1}$ but P_s suddenly drops from 1.0 to 0.5 pu at $t = 50\,s$. Accordingly, P_{DEG} also drops from around 0.25 to 0 pu. Surplus energy can be stored in FESS and CAES and both powers are around 0.2 pu. The Δf slightly rises above zero due to sudden load drop.

(3) *Sudden load rise*: When $100\,s < t < 200\,s$, V_W is still around $7.5\,m\,s^{-1}$ but P_s suddenly rises from 0.5 to 1.0 pu at $t = 100\,s$. The responses are similar to the ones for $0\,s < t < 50\,s$ since the studied system returns back to the same operating points of the base case.

(4) *Sudden drop of wind speed*: When $200\,s < t < 300\,s$, V_W suddenly drops to a low wind level at $t = 200\,s$ and P_{WTG} decreases to 0.1 pu but P_{WETG} is still around 0.3 pu. Since P_s is still kept at 1.0 pu, DEGs start up to generate P_{DEG} of around 0.6 pu. No surplus power can be stored in CAES and FESS and, hence, both P_{FESS} and P_{CAES} are equal to zero. The variation of Δf is very close to zero since the total generated power just matches the required power demand of the connected loads.

(5) *Performance comparison of using HVDC and HVAC*: When $0\,s < t < 300\,s$, both P_{WTG} and P_{WETG} are delivered to the connected loads through the HVDC link. Since the power loss of the HVDC link is lower than the one of the HVAC line, the DEGs may deliver less power to system. When $50\,s < t < 100\,s$, both FESS and CAES can store more energy for the system with the HVDC link than the one with the HVAC line. It is obviously seen from Fig. 7 that the quantities of P_T, P_{FESS}, P_{CAES}, and Δf for the system with the HVDC link are higher than the ones for the system with an HVAC line.

5.4. System without WTGs and WETGs

This subsection assumes that the WTGs and WETGs are both disconnected from the system and the time-domain simulation results are shown in Fig. 8.

When $0\,s < t < 300\,s$, the power generated by the WTGs or the WETGs is identically zero. The DEGs automatically start up and connect to the system at $t = 0\,s$ to supply P_{DEG} of about 0.8 pu to meet load demand. The P_{DEG} also drops from around 0.8 to 0.3 pu due to a sudden drop of P_s at $t = 50\,s$. Both energy storage systems can release about 0.2 pu to the connected loads to compensate the insufficient of power generation. The system frequency deviation Δf is varied slightly lower than zero since total power generation is small.

6. Frequency-domain simulation results

To further validate the analyzed time-domain simulated results, this section determines frequency-domain characteristics of the studied PG/ESS using eigenvalues and participation factors. These analyzed results are very useful to check small-signal stability of the studied hybrid PG/ESS under steady-state operation. According to the linearized state-space system equations derived in Section 2, the system eigenvalues of the studied system can be solved by the following equation:

$$\det(\lambda[I] - [A]) = 0 \tag{15}$$

where $\det(\cdot)$ denotes the determinant operation of '·', λ is one of the system eigenvalues, $[A]$ is the system matrix, and $[I]$ is an identity matrix having the same dimensions as $[A]$.

A participation matrix $[P]$ can be employed to identify the relationship between the selected state variables and the calculated eigenvalues of the studied system. The participation matrix combines both right and left eigenvectors of $[A]$ as a measure to analyze the association between state variables and eigenvalues. The participation matrix $[P]$ is expressed by

$$[P] = [\,p_1 \quad p_2 \quad \cdots \quad p_n\,] \tag{16}$$

in which

$$p_i = \begin{bmatrix} p_{1i} \\ p_{2i} \\ \vdots \\ p_{ni} \end{bmatrix} = \begin{bmatrix} \phi_1\psi_{i1} \\ \phi_{2i}\psi_{i2} \\ \vdots \\ \phi_{ni}\psi_{in} \end{bmatrix} \tag{17}$$

where ϕ_{ki} is the element on the kth row and ith column of the modal matrix $[\Phi]$ and it is also the kth entry of the right eigenvector ϕ_i while ψ_{ki} is the element on the ith row and kth column of the modal matrix $[\Psi]$ and it is also the kth entry of the left eigenvector Ψ_i.

Table 2
Eigenvalues (rad s^{-1}) of the studied hybrid PG/ESS

Case 1				Case 2			
With HVDC		Without HVDC		With HVDC		Without HVDC	
λ_1	−13.782	λ_1	−13.784	λ_1	−13.784	λ_1	−13.784
λ_2	−7.2629	λ_2	−7.2629	λ_2	−7.2629	λ_2	−7.2629
λ_3	−0.5529	λ_3	−0.5529	λ_3	−0.5529	λ_3	−0.5529
λ_4	−10.0	λ_4	−10.0	λ_4	−10.0	λ_4	−10.0
λ_5	−0.25	λ_5	−0.25	λ_5	−1.4286	λ_5	−0.6667
λ_6	−5.0	λ_6	−5.0	λ_6	−0.6667	λ_6	−0.5
λ_7	−1.4286	λ_7	−0.6667	λ_7	−0.5		
λ_8	−0.6667	λ_8	−0.50				
λ_9	−0.5						

The calculated participation matrices for the studied PG/ESS under Case 1 with the HVDC link, Case 1 without the HVDC link, Case 2 with the HVDC link, and Case 2 without the HVDC link using (16) and (17) are respectively listed as below.

$$\begin{array}{c}\begin{bmatrix} 0 & 0 & 0 & 0 & 0 & 0 & 0 & 1 & 0 \\ 0 & 0 & 0 & 0 & 0 & 0 & 0 & 0 & 1 \\ 0 & 0 & 0 & 0 & 0 & 0 & 1 & 0 & 0 \\ 0 & 0 & 0 & 0 & 0 & 1 & 0 & 0 & 0 \\ 0 & 0 & 0 & 0 & 1 & 0 & 0 & 0 & 0 \\ -0.0017 & -0.0046 & 1.0063 & -0.0000 & 0 & 0 & 0 & 0 & 0 \\ 0.0122 & 0.0169 & -0.0000 & 0.9709 & 0 & 0 & 0 & 0 & 0 \\ 0.4068 & 0.5647 & -0.0006 & 0.0291 & 0 & 0 & 0 & 0 & 0 \\ 0.5826 & 0.4230 & -0.0056 & -0.0000 & 0 & 0 & 0 & 0 & 0 \end{bmatrix} \begin{bmatrix} \Delta P_{\mathrm{WTG}} \\ \Delta P_{\mathrm{WETG}} \\ \Delta P_{\mathrm{HVDC}} \\ \Delta P_{\mathrm{AE}} \\ \Delta P_{\mathrm{FC}} \\ \Delta P_{\mathrm{DEG}} \\ \Delta P_{\mathrm{FESS}} \\ \Delta P_{\mathrm{CAES}} \\ \Delta f \end{bmatrix} \\ \begin{matrix} \lambda_1 & \lambda_2 & \lambda_3 & \lambda_4 & \lambda_5 & \lambda_6 & \lambda_7 & \lambda_8 & \lambda_9 \end{matrix} \end{array} \quad (18)$$

$$\begin{array}{c}\begin{bmatrix} 0 & 0 & 0 & 0 & 0 & 0 & 1 & 0 \\ 0 & 0 & 0 & 0 & 0 & 0 & 0 & 1 \\ 0 & 0 & 0 & 0 & 0 & 1 & 0 & 0 \\ 0 & 0 & 0 & 0 & 1 & 0 & 0 & 0 \\ -0.0017 & -0.0046 & 1.0063 & -0.0000 & 0 & 0 & 0 & 0 \\ 0.0122 & 0.0169 & -0.0000 & 0.9709 & 0 & 0 & 0 & 0 \\ 0.4068 & 0.5647 & -0.0006 & 0.0291 & 0 & 0 & 0 & 0 \\ 0.5826 & 0.4230 & -0.0056 & -0.0000 & 0 & 0 & 0 & 0 \end{bmatrix} \begin{bmatrix} \Delta P_{\mathrm{WTG}} \\ \Delta P_{\mathrm{WETG}} \\ \Delta P_{\mathrm{AE}} \\ \Delta P_{\mathrm{FC}} \\ \Delta P_{\mathrm{DFG}} \\ \Delta P_{\mathrm{FESS}} \\ \Delta P_{\mathrm{CAES}} \\ \Delta f \end{bmatrix} \\ \begin{matrix} \lambda_1 & \lambda_2 & \lambda_3 & \lambda_4 & \lambda_5 & \lambda_6 & \lambda_7 & \lambda_8 \end{matrix} \end{array} \quad (19)$$

$$\begin{array}{c}\begin{bmatrix} 0 & 0 & 0 & 0 & 0 & 1 & 0 \\ 0 & 0 & 0 & 0 & 0 & 0 & 1 \\ 0 & 0 & 0 & 0 & 1 & 0 & 0 \\ -0.0017 & -0.0046 & 1.0063 & -0.0000 & 0 & 0 & 0 \\ 0.0122 & 0.0169 & -0.0000 & 0.9709 & 0 & 0 & 0 \\ 0.4068 & 0.5647 & -0.0006 & 0.0291 & 0 & 0 & 0 \\ 0.5826 & 0.4230 & -0.0056 & -0.0000 & 0 & 0 & 0 \end{bmatrix} \begin{bmatrix} \Delta P_{\mathrm{WTG}} \\ \Delta P_{\mathrm{WETG}} \\ \Delta P_{\mathrm{HVDC}} \\ \Delta P_{\mathrm{DEG}} \\ \Delta P_{\mathrm{FESS}} \\ \Delta P_{\mathrm{CAES}} \\ \Delta f \end{bmatrix} \\ \begin{matrix} \lambda_1 & \lambda_2 & \lambda_3 & \lambda_4 & \lambda_5 & \lambda_6 & \lambda_7 \end{matrix} \end{array} \quad (20)$$

$$\begin{array}{c}\begin{bmatrix} 0 & 0 & 0 & 0 & 1 & 0 \\ 0 & 0 & 0 & 0 & 0 & 1 \\ -0.0017 & -0.0046 & 1.0063 & -0.0000 & 0 & 0 \\ 0.0122 & 0.0169 & -0.0000 & 0.9709 & 0 & 0 \\ 0.4068 & 0.5647 & -0.0006 & 0.0291 & 0 & 0 \\ 0.5826 & 0.4230 & -0.0056 & -0.0000 & 0 & 0 \end{bmatrix} \begin{bmatrix} \Delta P_{\mathrm{WTG}} \\ \Delta P_{\mathrm{WETG}} \\ \Delta P_{\mathrm{DEG}} \\ \Delta P_{\mathrm{FESS}} \\ \Delta P_{\mathrm{CAES}} \\ \Delta f \end{bmatrix} \\ \begin{matrix} \lambda_1 & \lambda_2 & \lambda_3 & \lambda_4 & \lambda_5 & \lambda_6 \end{matrix} \end{array} \quad (21)$$

Table 2 lists the eigenvalues of the studied PG/ESS with and without the HVDC link under the two studied cases. From the comparative results listed in Table 2, it is found that all system eigenvalues are located on the left half side of the complex plane and, hence, the studied system is stable when a small disturbance is applied.

It is found from the eigenvalues listed in the first column of Table 2 that Case 1 with HVDC has an eigenvalue of $\lambda_7 = -1.4286$ that corresponds to the state variable P_{HVDC}. The element of 1.0 at the 3rd row and the 7th column listed in the matrix [P] of Eq. (18) also confirm this point. The eigenvalue of $\lambda_5 = -0.25$ listed in Case 1 of Table 2 corresponds to the state variable P_{FC} and this mode is one of the system eigenvalues closest to the imaginary axis of the complex plane. This is due to the fact that the time constant of the FC $T_{\mathrm{FC}} = 4$ s that is the longest time constant in the studied PG/ESS under Case 1 regardless of the employment of the HVDC link.

It can also be determined from the eigenvalues listed in the third column of Table 2 that Case 2 with HVDC has an eigenvalue of $\lambda_5 = -1.4286$ that also corresponds to the state variable P_{HVDC}. The element of 1.0 at the 3rd row and the 5th column listed in the matrix [P] of Eq. (20) also confirm this point. The eigenvalue of $\lambda_7 = -0.5$ in the third column and $\lambda_6 = -0.5$ in the fourth column listed in Case 2 of Table 2 correspond to the state variable P_{WETG} and this mode is one of the system eigenvalues closest to the imaginary axis of the complex plane. This mode can affect the response time of the studied PG/ESS under Case 2 regardless of the employment of the HVDC link.

7. Conclusions

This paper has presented both time-domain and frequency-domain simulations for the analysis of a hybrid marine renewable-energy power generation/energy storage system connected to isolated loads through an HVDC link. The studied system contains wind-turbine generators, diesel-engine generators, fuel cells, and wave-energy turbine generators, a compressed air energy storage system, and a flywheel energy storage system. The required hydrogen for FCs is by means of an aqua electrolyzer whose required electric energy is supplied by a part of the generated power from WTGs and WETGs. The employed transfer functions for the WTGs, WETGs, DEGs, FCs, AE, FESS, and CAES are represented by first-order lag to simplify the tasks of system simulations. The models for wind speed, mechanical power of WTG, and wave height are also properly selected to simulate the important performance of the studied marine hybrid PG/ESS.

It can be concluded from the time-domain simulation results of the two studied cases that the power generation from WTGs, WETGs, DEGs, and FCs with FESS and CAES can effectively meet the sudden variations of the load power demand. The system frequency deviation can also be properly controlled to be within a very small range. In addition, the use the HVDC link can effectively reduce power transmission loss and decrease the use of fossil for DEGs. Frequency-domain characteristics of the studied PG/ESS using eigenvalues, and participation factors have

also been carried out to validate the stability of the studied PG/ESS under the two studied cases with and without the HVDC link.

References

[1] P. Bresesti, W.L. Kling, R.L. Hendriks, R. Vailati, HVDC connection of offshore wind farms to the transmission system, IEEE Trans. Energy Conv. 22 (1) (2007) 37–43.

[2] B.C. Ummels, M. Gibescu, E. Pelgrum, W.L. Kling, A.J. Brand, Impacts of wind power on thermal generation unit commitment and dispatch, IEEE Trans. Energy Conv. 22 (1) (2007) 44–51.

[3] J. Ribrant, L.M. Bertling, Survey of failures in wind power systems with focus on Swedish wind power plants during 1997–2005, IEEE Trans. Energy Conv. 22 (1) (2007) 167–173.

[4] J.C. Amphlett, R.F. Mann, B.A. Peppley, P.R. Roberge, A. Rodrigues, J. Power Sources 61 (1996) 183–188.

[5] Y.H. Li, S.S. Choi, S. Rajakaruna, An analysis of the control and operation of a solid oxide fuel-cell power plant in an isolated system, IEEE Trans. Energy Conv. 20 (2) (2005) 381–387.

[6] X.J. Liu, C.W. Chan, Control of a solid oxide fuel cell power plant in a grid-connected system, IEEE Trans. Energy Conv. 22 (2) (2007) 405–413.

[7] J.C. Amphlett, R.M. Baumert, R.F. Mann, B.A. Peppley, P.R. Roberge, A. Rodrigues, J. Power Sources 49 (1994) 349–356.

[8] A. Bilodeau, K. Agbossou, J. Power Sources 162 (2006) 757–764.

[9] P.S. Kauranen, P.D. Lund, J.P. Vanhanen, Int. J. Hydrogen Energy 18 (1993) 383–390.

[10] D.J. Hall, R.G. Colclaser, Transient modeling and simulation of a tubular solid oxide fuel cell, IEEE Trans. Energy Conv. 14 (3) (1999) 749–753.

[11] W.S. Fyfe, M.A. Powell, B.R. Hart, B. Ratanasthien, A global crisis: energy in the future, Nonrenewable Resour. (1993) 187–195.

[12] S.S. Yegna Narayanan, B.K. Murthy, G. Rao, Sridhara, Dynamic analysis of a grid-connected induction generator driven by a wave-energy turbine through hunting networks, IEEE Trans. Energy Conv. 14 (1) (1999) 115–120.

[13] D.R. Kiran, A. Palani, S. Muthukumar, V. Jayashankar, Steady grid power from Well energy, IEEE Trans. Energy Conv. 12 (1) (2007) 539–540.

[14] R.S. Weissbach, G.G. Karady, R.G. Farmer, Dynamic voltage compensation on distribution feeders using flywheel energy storage, IEEE Trans. Power Del. 14 (2) (1999) 465–471.

[15] D.J. Swider, Compressed air energy storage in an electricity system with significant wind power generation, IEEE Trans. Energy Conv. 22 (1) (2007) 95–102.

[16] T. Senjyu, T. Nakaji, K. Uezato, T. Funabashi, A hybrid power system using alternative energy facilities in isolated island, IEEE Trans. Energy Conv. 20 (2) (2005) 406–414.

[17] F. Valenciaga, P.F. Puleston, P.E. Battaiotto, Power control of a solar/wind generation system without wind measurement: a passivity/sliding mode approach, IEEE Trans. Energy Conv. 18 (4) (2003) 501–507.

[18] K. Rajashekara, Hybrid fuel-cell strategies for clean power generation, IEEE Trans. Ind. Appl. 41 (3) (2005) 682–689.

[19] E. Muljadi, H.E. McKenna, Power quality issues in a hybrid power system, IEEE Trans. Ind. Appl. 38 (3) (2002) 803–809.

[20] A. Emadi, S.S. Williamson, A. Khaligh, Power electronics intensive solutions for advanced electric, hybrid electric, and fuel cell vehicular power systems, IEEE Trans. Power Electron. 21 (3) (2006) 567–577.

[21] K. Agbossou, M. Kolhe, J. Hamelin, T.K. Bose, Performance of a stand-alone renewable energy system based on energy storage as hydrogen, IEEE Trans. Energy Conv. 19 (3) (2004) 633–640.

[22] P.F. Ribeiro, B.K. Johnson, M.L. Crow, A. Arsoy, Y. Liu, Energy storage systems for advanced power applications, IEEE Proc. 89 (12) (2001) 1744–1756.

[23] R. Dettmer, Revolutionary energy—a wind/diesel generator with flywheel storage, IEE Rev. 36 (4) (1990) 149–151.

[24] P.M. Anderson, A. Bose, Stability simulation of wind turbine system, IEEE Trans. Power Apparatus Syst. 102 (2) (1983) 3791–3795.

[25] F.A. Farret, M.G. Simões, Integration of Alternative Sources of Energy, Wiley-IEEE Press, New York, 2006.

[26] D.-J. Lee, L. Wang, Small-signal stability analysis of an autonomous hybrid renewable energy power generation/energy storage system, Part I: Time-domain simulations, IEEE Trans. Energy Conv. 32 (1) (2008) 311–320.